

Vertex effects in describing the ionization energies of the first-row transition-metal monoxide molecules

Yanyong Wang

CAS Key Laboratory of Quantum Information, University of Science and Technology of China, Hefei, Anhui 230026, China

Xinguo Ren*

Institute of Physics, Chinese Academy of Sciences, Beijing 100190, China and

Songshan Lake Materials Laboratory, Dongguan 523808, Guangdong, China

(Dated: August 30, 2022)

The GW approximation is considered to be the simplest approximation with Hedin's formulation of many-body perturbation theory. It is expected that some of the deficiencies of the GW approximation can be overcome by adding the so-called vertex corrections. In this work, the recently implemented $G_0W_0\Gamma_0^{(1)}$ scheme, which incorporates the vertex effects by adding the full second-order self-energy correction to the GW self-energy, is applied to a set of first-row transition-metal monoxide (TMO) anions. Benchmark calculations show that results obtained by $G_0W_0\Gamma_0^{(1)}$ on top of the B3LYP hybrid functional starting point (SP) are in good agreement with experiment data, giving a mean absolute error of 0.13 eV for a testset comprising the ionization energies (IEs) of 27 outer valence molecular orbitals (MOs) from 9 TMO anions. A systematic SP-dependence investigation by varying the ratio of the exact exchange (EXX) component in the PBE0-type SP reveals that, for $G_0W_0\Gamma_0^{(1)}$, the best accuracy is achieved with 20% EXX. Further error analysis in terms of the orbital symmetry characteristics (i.e., σ , π , or δ) in the testset indicate the best amount of EXX in the SP for $G_0W_0\Gamma_0^{(1)}$ calculations is independent of MO types, and this is in contrast with the situation of G_0W_0 calculations where the best EXX ratio varies for different classes of MOs. Despite its success in describing the absolute IE values, we however found that $G_0W_0\Gamma_0^{(1)}$ faces difficulties in describing the energy separations between certain states of interest, worsening the already underestimated G_0W_0 predictions.

I. INTRODUCTION

Among various electronic structure methods available in computational chemistry and materials science, the GW approximation (GWA) [1, 2] plays a central role in describing excitation energies in the one-electron attachment or detachment processes. Different from the Hartree-Fock theory, the GWA further accounts for the dynamic screening effects at the level of the random phase approximation (RPA), i.e., due to the creation of noninteracting electron-hole pairs as a linear response to the propagation of an external charge in an interacting electron cloud [3]. Exploiting the screening concept and error cancellations, the perturbative GW approach based on references provided by (generalized) Kohn-Sham density functional theory ((g)KS-DFT) [4–6] has achieved great success in its applications to weakly and moderately correlated systems [7–16]. Unsurprisingly, the GW approximation still suffers from a number of limitations [3, 16–18]. For example, it is known that one-shot G_0W_0 calculation had a dependence on the starting point (SP), i.e., the preceding (g)KS references [14–16, 19], which limits its reliability as a predictive method. This is particularly true for transition metal oxides (TMO): The G_0W_0 approach based on a (semi)local density functional may underestimate or even fail to predict the fundamental band gaps [20–22], while when starting from the DFT+ U or hybrid functional references, improvements can be achieved, but the results are still inconclusive [22–25]. The

self-consistent variant of the GWA, $scGW$, though satisfying some conserving laws, could lead to a substantial overestimation of the band gaps and bandwidths for periodic systems, as compared to experimental results [26–28], and in certain cases produces unphysical spectral properties [27–29]. For molecular systems, $scGW$ tends to underestimate the ionization energies (IEs) [30–33], and the deviations increase for larger organic molecules [15, 31].

Contributions from higher-order correlation effects, usually called the vertex corrections (VCs), is completely ignored in the GWA. This is partly because a direct evaluation of the diagrammatic three-point vertex function following the Hedin's equations are rather expensive. Theoretically, VCs are expected to remedy the defects and limitations of the GWA. In practice, most studies on VCs focus on devising simplified vertices to save computational cost. Nevertheless, VCs derived from a rigorous diagrammatic formulation are still of great interest and have the advantage that they can be applied to both finite and extended systems [34–39] unbiasedly. Technically, VCs can be added to either of the polarizability [40, 41] and the self-energy [42–44] or both [45, 46]. Recently, attempts have also been made towards incorporating the VCs within the self-consistency loop [45, 47–50]. It has been demonstrated that proper VCs can evidently improve the descriptions of band gaps [47, 49–51], IEs, and electron affinities (EA) [36, 43, 44]. Despite the impressive improvements achieved by including VCs in the screened Coulomb potential for bulk materials, a recent study [41] shows that an EOM-CCSD (equation-of-motion coupled-cluster with single and double excitations) conjectured polarizability that includes a diagrammatically based VC, deteriorates the description of

* renxg@iphy.ac.cn

IEs for a small set of molecules, compared to G_0W_0 . Recently, the present authors implemented the lowest-order vertex correction to the self-energy Σ in Hedin’s equations, corresponding to the full self-order self-energy (FSOS) in terms of W [44], and benchmarked its performance of small molecules composed of main-group elements. The resultant $G_0W_0\Gamma_0^{(1)}$ scheme, $\Sigma^{G_0W_0\Gamma_0^{(1)}} = \Sigma^{G_0W_0} + \Sigma^{\text{FSOS-}W_0}$, proves to be rather accurate in predicting IPs and EAs for such molecules [44], if PBE and PBE0 functionals are chosen as the starting points. However, the performance of $G_0W_0\Gamma_0^{(1)}$ for more complex molecules like those containing transition-metal (TM) atoms is still unknown.

In fact, even the performance assessment for GW are still largely limited to sp -electron systems in case of molecules, and only a few studies paid attentions to open-shell [48, 52] or strongly correlated ones [53–57]. Recently, Byun *et al.* [58] reported that a partial self-consistent GW approach, in which only the eigenvalues in G are updated, can achieve a fairly good agreement with experiment, but their calculations are limited to the early and late $3d$ -TMO anions. For $3d$ -TMO systems, a number of issues, like multiple close-lying excited spin states arising from the unpaired metal electrons, orbitals with different characteristics, hybridization and localization of orbitals to varying degrees, strong correlations of $3d$ -electrons, and multi-configurational nature of the wave function [59–63], all present substantial challenges to electronic structure calculation methods. For example, debates still exist concerning the ground state configurations and the assignments of the photoelectron spectra for some $3d$ -TMO anions [64–67]. In fact, in the past the ground states and the low-lying excited states of $3d$ -TMO clusters have been systematically studied by the high-level multireference methods [60, 67–72], DFT methods [61, 73, 74], and experimental anion photoelectron spectroscopy (PES) [64, 75–82]. In this work we study the vertex effects beyond the GWA in describing the charged excitations of the first-row transition-metal monoxide anions, and thereby we extend the assessment of the $G_0W_0\Gamma_0^{(1)}$ scheme to TMO molecules.

The rest of this paper is organized as follows: in Section II the computational settings and technical details are described. Then in Section III, the G_0W_0 and $G_0W_0\Gamma_0^{(1)}$ results on the ionization energies of low-lying states for the $3d$ -TMO testset will be presented and discussed. Here, special attention will be paid to the role of exact exchange (EXX) in the SPs, whereby the best amount of EXX before and after the inclusion of VCs in the computational schemes will be identified. A brief summary of this work will be given in Section IV.

II. COMPUTATIONAL DETAILS

The geometries of the $3d$ -TMO anions are optimized by KS-DFT within the Perdew-Burke-Ernzerhof (PBE) [83] generalized gradient approximation (GGA), which proves to be reliable for these systems [56, 61]. The FHI-aims-2020 *tier-2* numerical atomic orbital (NAO) basis sets for metal atoms and *tier-3* NAO basis set for the oxygen atom are used for ge-

ometry optimization calculations. Two different hybrid functionals, i.e., PBE0 [84] and B3LYP [85, 86] are used as the SPs for G_0W_0 and $G_0W_0\Gamma_0^{(1)}$ calculations. For molecules containing TM atoms, PBE0 is a fairly good choice for G_0W_0 calculations [53]. As the role of exact exchange (EXX) is crucial for systems with localized d orbitals, for comparison we will also test the popular B3LYP functional (with 20% EXX component), as well as the PBE0 family of functionals with varying EXX contributions as the SPs. For all the G_0W_0 and $G_0W_0\Gamma_0^{(1)}$ calculations, the Dunning’s augmented correlation-consistent “aug-cc-pV5Z” [87] Gaussian basis sets are used for all elements. Additionally, the modified Gauss-Legendre grid [88] with 240 points along the imaginary frequency axis is adopted to evaluate both the self-energy and the screened Coulomb interaction. As the self-energy is initially computed on the imaginary axis, an analytical continuation procedure is applied to transform the G_0W_0 or $G_0W_0\Gamma_0^{(1)}$ self-energy into the real axis using the Padé approximant [89] with 32 parameters. All the calculations are performed using the all-electron FHI-aims [88, 90] code package. The implementation details of $G_0W_0\Gamma_0^{(1)}$ in FHI-aims can be found in Ref. [44].

Besides $G_0W_0\Gamma_0^{(1)}$, an alternative beyond- GW scheme is the so-called second-order screened exchange (SOSEX) self-energy correction [42]. The SOSEX correlation self-energy can be viewed as an antisymmetrization of the correlation part of the GW self-energy by interchanging the way that the bare v line and the screened W line are connected in the Feynman diagram representation [42]. Previous studies show that, with the same SPs, $G_0W_0\Gamma_0^{(1)}$ and G_0W_0 +SOSEX yield similar IEs for main-group molecules [44]. As the testset is extended to $3d$ -TMO molecules where the presence of localized d -electrons poses additional challenges, it would be interesting to check if the similar performance still persists for these systems.

III. RESULTS AND DISCUSSIONS

In this section, we will present the main results of the present study, aiming at assessing the performance of G_0W_0 and $G_0W_0\Gamma_0^{(1)}$ for TMO molecules. To this end, we first introduce the $3d$ -TMO testset adopted in this work. As will be detailed below, the testset consists of 27 low-lying valence IEs from 9 TMO anions, where reliable experimental data are available. The performance of the G_0W_0 and $G_0W_0\Gamma_0^{(1)}$ approaches for describing the IEs of low-lying molecular states of the $3d$ -TMO anions will be analyzed through the mean errors (MEs) and mean absolute errors (MAEs) with reference to experimental reference values. Special attention will be paid to the SP dependence of the G_0W_0 and $G_0W_0\Gamma_0^{(1)}$ calculations. Specifically, we will monitor how the results change by varying the ratio of the EXX component in the preceding hybrid functional calculations.

TABLE I. Low-lying occupied MOs in the $3d$ -TMO anion orbital testset (denoted as TMO27), whose IEs are used to benchmark the theoretical methods in this work. The experimental reference IEs (in eV) are provided for the selected MOs of each TMO anion.

system	# of orbitals	experimental IE (eV) ^a									
		9σ	4π	$10\sigma_\alpha$	$9\sigma_\alpha$	$9\sigma_\beta$	$1\delta_\alpha$	$1\delta_\beta$	$4\pi_\alpha$	$4\pi_\beta$	$3\pi_\beta$
ScO ⁻	1	1.35									
TiO ⁻	3				1.73	1.30	2.00				
VO ⁻	3				1.93	1.23	2.40				
CrO ⁻	3				2.13		2.64		1.12		
MnO ⁻	2					1.38					3.58
FeO ⁻	5				2.36	1.50	3.39	1.98	2.56		
CoO ⁻	4				2.17	1.54		1.45	2.30		
CuO ⁻	2	2.75	1.78								
ZnO ⁻	4			2.09		3.89			2.71	2.40	

^a Experimental IE values are taken from: Ref. [75] for ScO⁻, Ref. [76] for TiO⁻, Ref. [77] for VO⁻, Ref. [91] for CrO⁻, Ref. [92] for MnO⁻, Ref. [93] for FeO⁻, Ref. [78] for CoO⁻, Ref. [80] for CuO⁻, and Ref. [82] for ZnO⁻, respectively.

A. The TMO27 testset

In Table III, we assemble a total of 27 frontier MOs, corresponding to selected low-lying molecular states of the first-row TMO anions. These energy levels have unambiguous MO assignments, established via a comparative analysis of their experimental PES spectra and theoretical calculations. The symmetry characteristics of these MOs are explicitly given in Table III. For notational convenience, below we shall term this testset as ‘‘TMO27’’. Except for ScO⁻ and CuO⁻, all other TMO anions have open-shell electronic structures. Specifically, TMO27 contains 14 σ -orbitals, 7 π -orbitals and 6 δ -orbitals, belonging to either up- or down-spin channels. The experimental IE values for these orbitals, taken from experimental literature [75–78, 80, 82, 91–93] and used as the reference data in the present work, are given in Table III.

Although these diatomic TMO anions are small in size and simple in chemical formula, they are in fact an important class of systems suitable for benchmarking the performance of theoretical methods. As mentioned in Sec. I, it is the competitions between $3d$ - and $4s$ -orbitals and the strong correlations among the $3d$ electrons that give rise to the complexity of the electronic structure of TMO systems. For mid-row TMO systems, as the number of $3d$ -electrons increases, the amount of electronic spin states grows quickly in a narrow energy window, which are manifested in their experimental spectral features. This inevitably increases the difficulty in assigning the PES peaks to the theoretically calculated energy levels. In fact, identifying the peaks in PES with single-electron detachment processes, and associating these with MO energy levels are not entirely trivial. In the Appendix, we give more details about how these issues are clarified in several prototypical TMO anions such as CrO⁻, MnO⁻ and CoO⁻.

B. Performance of G_0W_0 , $G_0W_0\Gamma_0^{(1)}$, and G_0W_0 +SOSEX

We performed G_0W_0 , $G_0W_0\Gamma_0^{(1)}$, and G_0W_0 +SOSEX calculations for nine TMO anions using computational setups described in Sec. II. The calculations were done on top of two popular hybrid functional (PBE0 and B3LYP) starting points. Due to the large self-interaction error in systems containing TM elements [55, 94], the commonly used PBE functional is not a proper SP. As a matter of fact, tentative calculations indicate that, for both G_0W_0 and $G_0W_0\Gamma_0^{(1)}$ calculations with the PBE SP, it’s rather hard and often impossible to obtain converged quasiparticle (QP) values when solving the QP equation iteratively, due to the complex structure of the self-energy near the solution.

1. FeO⁻: A case study

A general procedure of our study proceeds as follows: (1) Identify the ground-state (many-electron) configuration of the anions; (2) analyze the experimental PES and interpret the individual peaks in PES in terms of the single-particle detachment processes from the anions’ ground state; and (3) associate the experimental peak positions with the calculated QP energy levels, characterized by MO symmetries as listed in Table III. We have performed such analyses for all nine TMO anions. Below, using the FeO⁻ anion as a showcase, we illustrate how the entire calculation and analysis are carried out. To avoid redundancy, we will not describe other anions in detail here, but provides in the Appendix additional information for the cases where the analyses are not entirely trivial, such as CrO⁻, MnO⁻, and CoO⁻. Note that although multi-configurational characters are expected to be reflected in the anion PES of TMO systems, the primary peaks can be properly described by single particle excitations [64], and the ground-state wave function is supposed to be dominated by a

TABLE II. Ionization energies (in eV) of low-lying states in FeO^- , with its ground state established as ${}^4\Delta$ ($9\sigma^2 1\delta^3 4\pi^2$). After an electron is kicked out from one the MOs listed in the second row, the system becomes charge neutral and resides in a corresponding electronic state (final state) given in the first row.

Final state	${}^5\Delta$	${}^5\Sigma^+$	${}^3\Delta$	${}^3\Pi$	${}^3\Sigma^+$	${}^5\Phi$
MO	$9\sigma_\beta$	$1\delta_\beta$	$9\sigma_\alpha$	$4\pi_\alpha$	$1\delta_\alpha$	$3\pi_\beta$
Expt ^a	1.50	1.98	2.36	2.56	3.39	
PBE0	-0.20	0.77	1.20	1.26	2.69	2.38
	@PBE0					
G_0W_0	1.15	1.69	2.41	2.37	3.64	3.61
$G_0W_0+\text{SOSEX}$	-	2.36	2.61	2.85	4.01	3.89
$G_0W_0\Gamma_0^{(1)}$	1.63	2.29	2.65	2.73	3.95	3.96
B3LYP	-0.33	0.36	0.88	0.96	2.08	2.20
	@B3LYP					
G_0W_0	1.03	1.29	2.08	2.08	3.06	3.40
$G_0W_0+\text{SOSEX}$	-	2.01	2.25	2.51	3.41	3.67
$G_0W_0\Gamma_0^{(1)}$	1.55	1.90	2.33	2.42	3.36	3.76

^a Ref. [93].

single Slater determinant [61, 74, 95]. When there are controversies in the spectral assignments, we have to make a judicious decision based on our own calculation results.

The first step is to identify the ground-state configuration of FeO^- anion, i.e., how the outer valence MOs are occupied by electrons, which further determines the symmetry and spin moment of the system. In case of FeO^- anion, various experiments consistently confirm that the low-spin ($S = 3/2$) state ${}^4\Delta$ ($9\sigma^2 1\delta^3 4\pi^2$) is the ground state [64, 66, 96, 97], while multipreference and correlation calculations suggest the high-spin ($S = 5/2$) ${}^6\Sigma^+$ state ($9\sigma^2 4\pi^2 1\delta^2 10\sigma^1$) [65, 67] as the ground state. DFT studies (including PBE calculations in this work) in fact support the ${}^4\Delta$ proposal [61, 98, 99], in agreement with experiment. In Table II, we provide an orbital analysis of the experimental data, based on the assumption that ${}^4\Delta$ is the ground state of the anion, and the calculated results using hybrid functionals, G_0W_0 , and beyond- G_0W_0 approaches. After one electron is removed from the valence orbitals as given in the second row of Table II, the system becomes a neutral FeO molecule, with an electronic configuration (the final state) characterized by the symmetry symbols presented in the first row.

After the initial ground state of the anion is established, there is still the issue of assigning the spectral features to the final states with one electron removed, which directly corresponds to the energy ordering of the MOs (the second row in Table II) The original assignment of the spectral feature is based on relatively rough configuration interaction (CI) calculations in the early days [64, 100], while our proposed assignment chiefly follows the ordering of energy levels from hybrid functional calculations. In fact, the experimental assignment for the first two quintet states (${}^5\Delta$ and ${}^5\Sigma^+$) are fairly solid [64, 66, 101], and the difference between our assignment and that of Refs. [64, 100] is the ordering of the three triplet

states (${}^3\Delta$, ${}^3\Pi$ and ${}^3\Sigma^+$) in Table II. Based on the new spectra assignment, for the five peaks in the PES spectra of FeO^- anion [93], $G_0W_0\Gamma_0^{(1)}$ @B3LYP gives the best MAE with 0.07 eV, followed by G_0W_0 @PBE0 which also yields a rather good MAE of 0.23 eV. The high accuracy of the $G_0W_0\Gamma_0^{(1)}$ @B3LYP (also $G_0W_0+\text{SOSEX}$ @B3LYP) predictions for the spectra is a strong evidence supporting our assignment.

From Table II, we can see that the G_0W_0 method is problematic in predicting the ordering of $9\sigma_\alpha$ and $4\pi_\alpha$ -orbitals. In contrast, both $G_0W_0+\text{SOSEX}$ and $G_0W_0\Gamma_0^{(1)}$ restore the right energy ordering, and produce a separation between these two orbitals that compare well with the experimental results. Another interesting feature is that the $1\delta_\alpha$ orbital is rather sensitive to the SPs as compared to other orbitals. Changing the SP from B3LYP to PBE0 greatly raises (~ 0.6 eV) the calculated IE of $1\delta_\alpha$ -electron, bringing it close to the IE of $3\pi_\beta$ -electron and rendering the assignment of $1\delta_\alpha$ and $3\pi_\beta$ complicated with all the calculation results obtained with the PBE0 SP. More calculations in subsection III C reveal that the positions of δ -orbitals are very sensitive to the EXX amount. While with the B3LYP SP, the $1\delta_\alpha$ and $3\pi_\beta$ -orbitals are well separated, with both $G_0W_0+\text{SOSEX}$ and $G_0W_0\Gamma_0^{(1)}$ predicting a very accurate IE for the $1\delta_\alpha$ -electron.

2. Overall performance for TMO27

In Fig. 1, we plot the mean errors (ME) and mean absolute errors (MAE) of the calculated IE results of the low-lying states in the TMO27 testset, with respect to the experimental values for each individual anion. In fact, for ScO^- , there is just one MO (9σ) included, while for others, the results are an averaging of the (absolute) errors of 2-5 orbitals included in the testset (cf. Table III). The actual computational and experimental IE values for all the 27 MOs are presented in the supplementary material (SM). Similar to the case of main-group molecules, G_0W_0 has a general tendency to underestimate the IEs, although the magnitude of the underestimation depends on the SPs. It can be seen from Table III that G_0W_0 @PBE0 shows a better performance than G_0W_0 @B3LYP, reducing the MAE from 0.48 eV to 0.30 eV. Figure 1 further reveals that this is because G_0W_0 @PBE0 gives higher IEs than G_0W_0 @B3LYP, bringing the results in better agreement with experiment.

TABLE III. The MEs and MAEs (in eV) of the G_0W_0 , $G_0W_0+\text{SOSEX}$, and $G_0W_0\Gamma_0^{(1)}$ results on the IEs of the TMO27 testset with respect to experimental results.

SP	G_0W_0		$G_0W_0+\text{SOSEX}$		$G_0W_0\Gamma_0^{(1)}$	
	ME	MAE	ME	MAE	ME	MAE
@PBE0	-0.25	0.30	0.23	0.36	0.16	0.23
@B3LYP	-0.48	0.48	0.00	0.19	-0.06	0.13

Upon including the VCs, $G_0W_0\Gamma_0^{(1)}$ produces higher IEs than G_0W_0 , reducing the deviations between the computa-

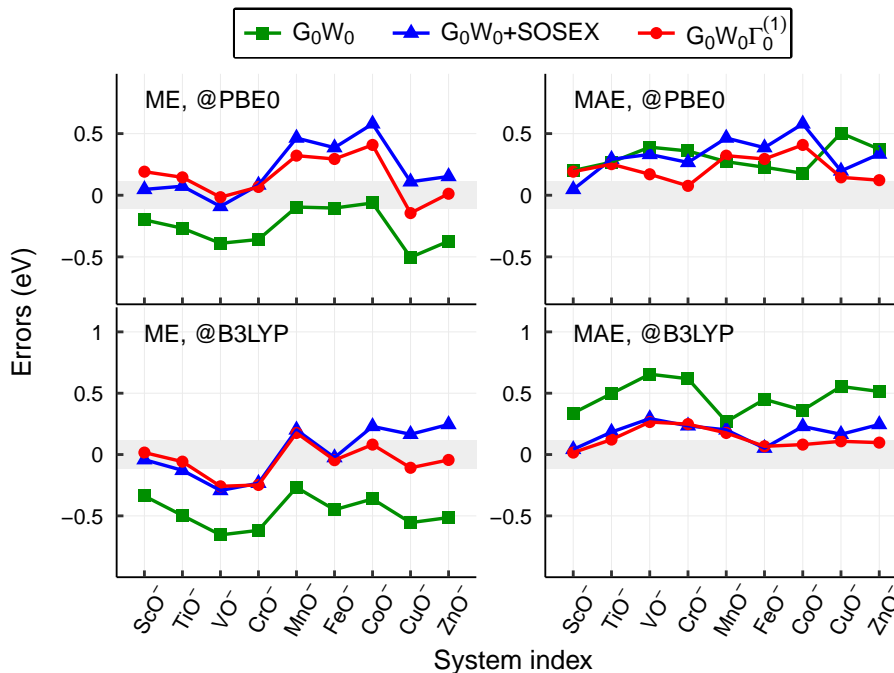


FIG. 1. The MEs (left panels) and MAEs (right panels) of the G_0W_0 , G_0W_0 +SOSEX, and $G_0W_0\Gamma_0^{(1)}$ results on the TMO27 test set. The correspondent SPs are labelled in each panel. The light grey area refers to the $[-0.1, 0.1]$ eV error window.

tional results and the experimental reference values, as can be clearly seen from the left panels of Fig. 1. Roughly speaking, the ME lines of $G_0W_0\Gamma_0^{(1)}$ follow the same variation pattern as the G_0W_0 ones with the same SPs, suggesting that the major effect of the VCs is to push the occupied frontier orbitals downwards to higher binding energies. The MAE results presented in Fig. 1 and Table III also show that, compared to G_0W_0 , the vertex corrections in both SOSEX and FSOS schemes systematically improve the agreement with experiment for the description of low-energy excited states. Particularly, $G_0W_0\Gamma_0^{(1)}$ @B3LYP gives the lowest MAE of 0.13 eV for the TMO27 testset. Interestingly, both G_0W_0 +SOSEX and $G_0W_0\Gamma_0^{(1)}$ calculations perform better on top of B3LYP than PBE0, while the opposite is true for G_0W_0 . Such a general behavior is observed for nearly all individual systems, except for CrO^- which is the only system for which PBE0 is a better SP than B3LYP for $G_0W_0\Gamma_0^{(1)}$ calculations, and for CuO^- and ZnO^- where the PBE0 and B3LYP SPs yield similar results.

Regarding the two VC schemes, the behavior of G_0W_0 +SOSEX generally follows that of $G_0W_0\Gamma_0^{(1)}$, as indicated by the ME and MAE curves in Fig. 1. It should be noted that the G_0W_0 +SOSEX data is absent for $9\sigma_\beta$ -electrons, due to the problem that a stable solution cannot be found by iteratively solving the QP equation. Quantitatively, $G_0W_0\Gamma_0^{(1)}$ still performs better than G_0W_0 +SOSEX, as can be seen from Table III. Figure 1 further reveals that the differences between these two VC schemes are more pronounced with the PBE0 SP than the B3LYP SP, and that the deviations are larger for late TMO anions, with $G_0W_0\Gamma_0^{(1)}$ yielding smaller errors.

3. Energy splitting

TABLE IV. Energy separations (in eV) of the two lowest spin states (i.e., the splitting between the HOMO and HOMO-1 level) in VO^- and TiO^- . Theoretical results are calculated with B3LYP, PBE0, G_0W_0 , and $G_0W_0\Gamma_0^{(1)}$, respectively.

	Expt ^a	B3LYP	@B3LYP		@PBE0		
			G_0W_0	$G_0W_0\Gamma_0^{(1)}$	PBE0	G_0W_0	$G_0W_0\Gamma_0^{(1)}$
VO^-	0.70	0.54	0.50	0.21	0.69	0.65	0.38
TiO^-	0.43	0.25	0.23	0.09	0.31	0.28	0.11

^a Experimental data for the TiO^- and VO^- anions are taken from Refs. [76] and [77], respectively.

In the above subsection, the overall performance of G_0W_0 , G_0W_0 +SOSEX, and $G_0W_0\Gamma_0^{(1)}$ based on two hybrid functional SPs are discussed. However, there are important properties which are not reflected in the above overall assessment, namely, the energy ordering and spacing between adjacent MOs. In Refs. [42, 44], we have pointed out that the description of the energy separation between the HOMO-1 and HOMO-2 MOs for the benzene molecule is rather challenging for G_0W_0 -based methods. For TMO anions, there has also been considerable interest in the energy spacing between the two lowest spin-states in VO^- [74, 102, 103]: the $^4\Sigma^-$ and $^2\Sigma^-$ states, which correspond to the detachments of $9\sigma_\beta$ -electron (located at the HOMO level) and $9\sigma_\alpha$ -electron (located at the HOMO-1 level) from the anion ground state $^3\Sigma$ (with an electronic configuration $9\sigma^21\delta^2$), respectively.

Table IV shows that hybrid functionals, in particular PBE0, produce an energy separation between $9\sigma_\alpha$ and $9\sigma_\beta$ states that compares fairly well with the experimental value. When G_0W_0 is applied on top, the energy splitting gets slightly reduced, unfortunately in the wrong direction, compared to the experimental value. Now, after further including the FSOS correction, the energy splitting gets seriously underestimated, resulting in a separation that is only half (in case of PBE0 SP) or even less (B3LYP SP) of the experimental counterpart (cf. the $G_0W_0\Gamma_0^{(1)}$ values in Table IV). To have a closer look at what happens, we plot in Fig. 2 the calculated IEs for both $9\sigma_\alpha$ and $9\sigma_\beta$ electrons, as determined by the hybrid functionals, G_0W_0 , and $G_0W_0\Gamma_0^{(1)}$. Figure 2 reveals that $G_0W_0\Gamma_0^{(1)}$ indeed gives the best absolute IE values compared to experiment, whereas both hybrid functionals and G_0W_0 show appreciable underestimation. However, for the latter two types of approaches, the IEs for the two states are underestimated by about the same amount, and thus the energy separation between the two states come out roughly right. In case of $G_0W_0\Gamma_0^{(1)}$, although the IE of $9\sigma_\beta$ is accurately predicted, that of $9\sigma_\alpha$ is underestimated by a few tens of meV, resulting in an overall underestimation of the energy separation. In fact, similar results with $G_0W_0\Gamma_0^{(1)}$ are also found in the case of TiO^- for the energy separation between its HOMO and HOMO-1 states. In Table IV, we list the energy separations given by the calculation methods at different levels for TiO^- and VO^- , which shows that the best prediction is given by PBE0 functional for both systems. When including the VCs, $G_0W_0\Gamma_0^{(1)}$ yields energy separations that are only about half of the G_0W_0 results. Varying the SPs does not remedy this problem. This study reveals that although $G_0W_0\Gamma_0^{(1)}$ improve over hybrid functionals and G_0W_0 regarding the determination of absolute energy positions of MOs of TMO anions, it is necessarily so for energy separations between these MOs, in particular between different spin states. Finally, we would like to mention that the G_0W_0 +SOSEX scheme, although performing well for benzene, yields even worse results than $G_0W_0\Gamma_0^{(1)}$ for the energy separations for TiO^- and VO^- . This problem needs further studies to achieve a better understanding.

C. Influence of the amount of EXX in the hybrid functional SPs

In this subsection, we devote ourselves to discussing the impact of the amount of EXX in the hybrid functional SPs on the accuracy of the subsequent G_0W_0 and beyond- G_0W_0 calculations. In the previous section, we have observed that, out of the two hybrid functionals, G_0W_0 performs better with the PBE0 SP, whereas G_0W_0 +SOSEX and $G_0W_0\Gamma_0^{(1)}$ perform better with the B3LYP SP. One of the major differences between PBE0 and B3LYP is the ratio of EXX they contain: In PBE0, there is 25% EXX, while in B3LYP, there is 20% EXX. To check if it is the different ratio of EXX in these two hybrid functionals that caused the difference, we carried out a systematic investigation by varying the ratio of EXX in the PBE0

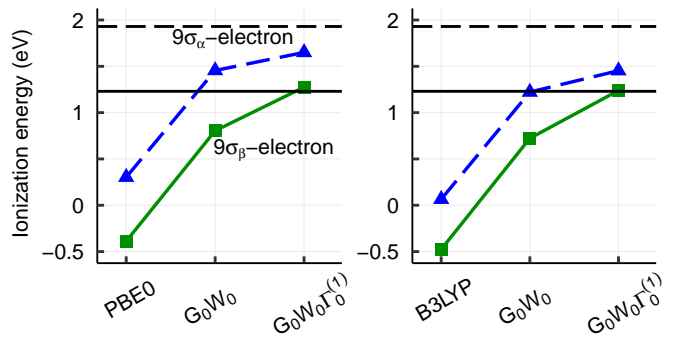


FIG. 2. The IEs of the two lowest spin orbitals in the VO^- anion as predicted by hybrid functional calculations, G_0W_0 and $G_0W_0\Gamma_0^{(1)}$ with corresponding SPs. The dashed and solid lines correspond to the ionization of the $9\sigma_\alpha$ and $9\sigma_\beta$ -electrons respectively, while the experimental values for $9\sigma_\alpha$ and $9\sigma_\beta$ -electrons are marked by horizontal dashed and solid lines.

functional from 15% to 60%, and monitor how the performance changes. The second motivation of this investigation is to check if the improvement brought by the VCs seen in Sec. III B 2 can be achieved by G_0W_0 on top of a better SP.

Specifically, we performed G_0W_0 , G_0W_0 +SOSEX and $G_0W_0\Gamma_0^{(1)}$ calculations for the TMO27 testset based on the PBE0-type hybrid functionals with the EXX ratio α varying from 0.15 to 0.60, each separated by an interval 0.05. The MEs and MAEs of the obtained IE results of the three methods with respect to the experimental reference values are plotted in Fig. 3 as a function of α . From the left (ME) panel of Fig. 3, one can see that as α increases, the IE values obtained by all three methods increase steadily, first approaching, and then exceeding and departing from the reference values. The actual calculated IE values for individual anions for all α 's can be found in the SM. For a given α , the G_0W_0 +SOSEX and $G_0W_0\Gamma_0^{(1)}$ IE's are always higher than the G_0W_0 counterpart, and the ME curves of the former are almost a constant upward shift (i.e., roughly independent of α) of the latter. Comparing the two VC schemes, the ME curves of G_0W_0 +SOSEX and $G_0W_0\Gamma_0^{(1)}$ are nearly on top of each other. One may further notice that there is a kick in the ME curves (and also in the MAE curves in the right panel) at around $\alpha = 0.45$. The underlying reason for this behavior is that the ground state of FeO^- is incorrectly predicted by PBE0 calculations with $\alpha > 0.40$, and thereby further PES assignment is meaningless. Moreover, in the valid regime of α , the FeO^- results are more sensitive to the amount of EXX than other systems, hence contributing a significant part to the slope of the ME curves. For $\alpha > 0.40$, the FeO^- data are excluded, and this results in a noticeable drop of the slope of the ME (MAE) curves.

In the right panel of Fig. 3, we plotted the MAEs of the three schemes as a function of α . The minima of MAE lines signify the best α for each method. The MAE curves show that, for G_0W_0 calculations, the PBE0 with 30% EXX provides the best SP, whereas for both G_0W_0 +SOSEX and $G_0W_0\Gamma_0^{(1)}$ calculations the best fraction of EXX is 20%. Furthermore, one can see that the minimum of $G_0W_0\Gamma_0^{(1)}$'s MAE line is lower

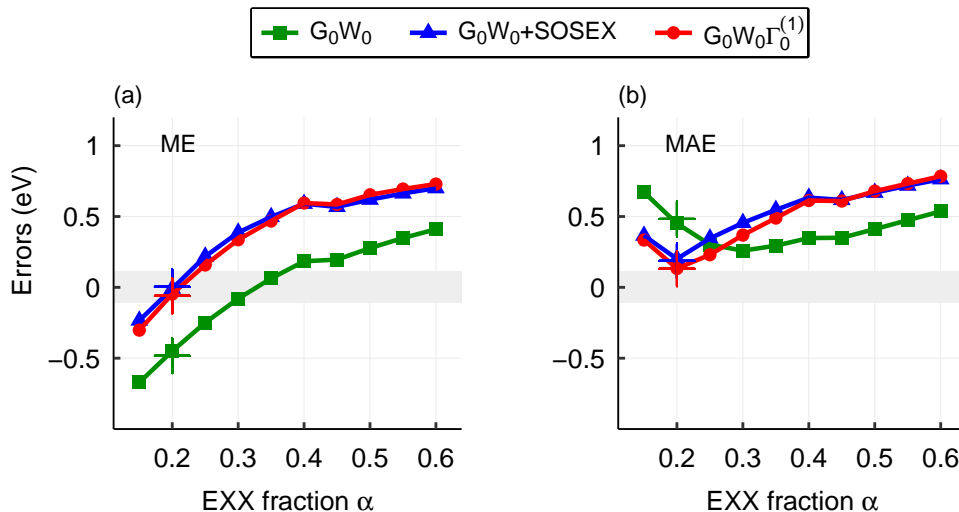


FIG. 3. MEs (left panel) and MAEs (right panel) of the G_0W_0 , G_0W_0 +SOSEX and $G_0W_0\Gamma_0^{(1)}$ results on the IEs of low-lying states for the TMO27 testset when varying the EXX ratio from 0.15 to 0.60 in the PBE0-type functional. Additionally, the corresponding G_0W_0 and beyond- G_0W_0 results obtained with the B3LYP SP (which has 20% EXX) are labeled with crosses.

than that of G_0W_0 's, meaning that with VCs, one can achieve an accuracy (MAE of 0.13 eV for $G_0W_0\Gamma_0^{(1)}$) that cannot be achieved by G_0W_0 with best tuned SP (MAE of 0.26 eV for G_0W_0). For comparison, we also marked in Fig. 3 the ME and MAE results obtained with the B3LYP SP at the EXX ratio of 0.2, where one can see that very similar accuracy is achieved for all three methods on top of the B3LYP SP and on top of the PBE0-type functional with 0.2 EXX.

What Fig. 3 shows is the overall behavior of the SP dependence of the three methods for the entire TMO27 testset. As described in Sec. III A, this testset consists of 14 σ -orbitals, 7 π -orbitals, and 6 δ -orbitals. It would be interesting to check if there is any difference in the SP dependence of these three different types of MOs. To this end, in Fig. 4 we plot the ME and MAEs of the three methods separately for the σ , π , and δ types of MOs. Firstly, from the ME curves in the upper panels of Fig. 4, one can clearly see that the three subsets with different orbital characters show rather different dependence on the fraction of EXX α . The degree of sensitiveness grows from σ to π , and to δ . This indicates that simply adjusting the ratio of EXX may not be sufficient to reach the best description for all the orbital types, limiting the achievable accuracy at the G_0W_0 level. Indeed, the MAE lines in the lower panels in Fig. 4 indicate that the best amount of EXX in PBE0-type SP for G_0W_0 is 0.45 for σ -orbitals, 0.35 for π -orbitals, and 0.30 for δ -orbitals, respectively. Interestingly, for $G_0W_0\Gamma_0^{(1)}$ the MAE lines reach minima at a common EXX ratio of 0.20 for all the three MO types, and for G_0W_0 +SOSEX, $\alpha = 0.20$ is also the best for π - and δ -orbitals. However, for the σ orbitals, the G_0W_0 +SOSEX MAE curve is rather flat and does not show a noticeable dependence on α in a wide range from 0.2 to 0.6. For clarity these results are also summarized in Table V. By classifying the results with regard to different orbital types, the distinction between different methods becomes clearer. For example, Fig. 4 shows the evolution of the MAEs

as a function of the EXX ratio for two VC schemes are rather close for δ -orbitals, while noticeable difference exists for α - and π -orbitals. Finally, we again marked the B3LYP results in Fig. 4, from which one can see similar accuracy is obtained for all three orbital types for the three methods based on B3LYP and the PBE0 with 20% EXX.

TABLE V. The minimal MAEs (in eV) and the corresponding optimal EXX ratios in the PBE0 SP for the G_0W_0 , G_0W_0 +SOSEX, and $G_0W_0\Gamma_0^{(1)}$ methods in predicting IEs in the three subsets (σ , π , and δ) of the TMO27 testset.

Method	σ -electrons		π -electrons		δ -electrons	
	MAE	EXX	MAE	EXX	MAE	EXX
G_0W_0	0.22	45%	0.23	35%	0.23	30%
G_0W_0 +SOSEX	0.25	30%	0.18	20%	0.12	20%
$G_0W_0\Gamma_0^{(1)}$	0.14	20%	0.14	20%	0.11	20%

IV. CONCLUSION

In summary, we have performed a detailed study of the vertex effect in beyond- G_0W_0 schemes for describing the outer valence IEs of $3d$ -TMO anions. Using a testset comprising 27 MOs, we demonstrate that including the vertex corrections within schemes like $G_0W_0\Gamma_0^{(1)}$ is advantageous and yields an accuracy that cannot be achieved by simple G_0W_0 schemes. A comprehensive study of the influence of the amount of EXX contributions in the hybrid functional SPs shows that the $G_0W_0\Gamma_0^{(1)}$ scheme performs best at a ratio of 20% for all types of MOs with different symmetries (α , π , or δ) characteristics, whereas for G_0W_0 , generally a higher fraction is preferred, and the best amount varies for different types of MOs. However, although vertex corrections lead to better absolute IEs for

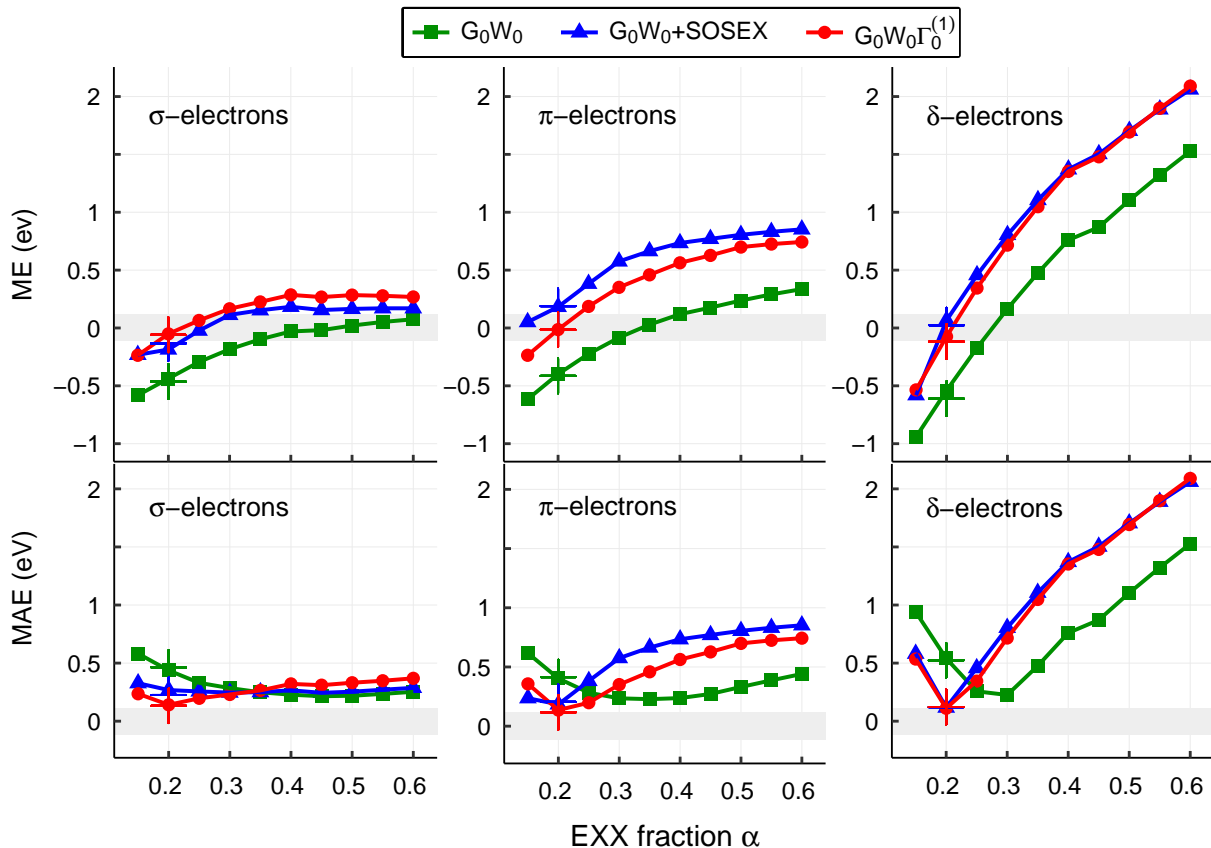


FIG. 4. MEs (upper panels) and MAEs (lower panels) of the G_0W_0 , G_0W_0 +SOSEX and $G_0W_0\Gamma_0^{(1)}$ results on the IEs of σ - (left panels), π - (middle panels) and δ -orbitals (right panels), respectively, in the TMO27 testset when varying EXX ratios from 0.15 to 0.60 in the PBE0 SP. In addition, the corresponding G_0W_0 and beyond- G_0W_0 results on top of B3LYP are labeled with crosses.

TMO anions, both G_0W_0 +SOSEX and $G_0W_0\Gamma_0^{(1)}$ can deteriorate the description of energy separations between adjacent MOs, like those in VO^- and TiO^- , compared to G_0W_0 and the hybrid functionals. More investigations are still needed for a better understanding of this issue.

DATA AVAILABILITY

The data that supports the findings of this study are available within the article and its supplementary material.

ACKNOWLEDGMENTS

This work is supported by National Natural Science Foundation of China (Grant Nos. 12134012, 11874335, 12188101), and The Max Planck Partner Group for *Advanced Electronic Structure Methods*.

Appendix A: Clarification on the one-electron PES assignment

As mentioned in Sec. III A and III B 1, the assignment of the experimental PES spectral features to one-electron removal

energies requires special attentions. Below we provide more information about this aspect for CrO^- , MnO^- , and CoO^- .

1. CrO^-

A key step in the spectral assignment is to identify the ground-state (and in certain cases relevant metastable-state) electronic configurations from which the electrons are removed. For CrO^- , it has been observed that, in the anion PES experiments, the plentiful spectral features is a blending of photoelectrons emitted from its anion ground state and a metastable anion state [91, 92]. Our PBE calculation indicates that the high-spin state ${}^6\Sigma^+$ with the electronic configuration $9\sigma^1 4\pi^2 1\delta^2$ as the ground state of CrO^- , consistent with previous GGA studies [61]. Additional PBE0 calculation also support this result, with a minor difference of 0.0013 Å on the bond length obtained by the two functionals. Further PBE calculations suggest that, the low-spin ${}^4\Pi$ state of CrO^- is 0.125 eV higher than ${}^6\Sigma^+$ in total energy, agreeing well with the experimental separation of 0.096 eV [91]. As mentioned above, the identification of the anion ground state is important for the subsequent QP calculations, as the spectral assignment is established between the PES peaks and the QP energy levels of the anion ground state, which ultimately determines

the performance of the G_0W_0 method and VC schemes. After the initial state is pinpointed, the energy ordering of individual single-particle orbitals still needs to be sorted out. In this regard, two different assignments have been proposed for CrO^- : one is based on Δ -SCF calculations with GGA functionals [91], and the other is the high-level complete-active-space self-consistent-field/multireference configuration interaction (CASSCF/MRCI) calculations [104]. The orbital ordering predicted by our hybrid functional calculations is in line with the CASSCF/MRCI results [104], and therefore we adopt their assignment. One of the essential difference between these two calculation results is the relative positions of $9\sigma_\alpha$ and $1\delta_\alpha$ orbitals: GGA predicts the $1\delta_\alpha$ orbital lies higher than $9\sigma_\alpha$ [91] (agreeing with our own PBE calculation) while the order is reversed in MRCI calculations [104] (agreeing with our hybrid functional calculation results). In fact, the $1\delta_\alpha$ -orbital always lies lower than $9\sigma_\alpha$ orbital in the other $3d$ -TMO anions with unambiguous assignments of their anion PES spectra. On the other hand, we believe that EXX is crucial in predicting the correct ordering of the frontier orbitals in CrO^- , as five parallel-spin electrons in the ${}^6\Sigma^+$ state could lead to larger exchange interactions.

2. MnO^-

In the original anion PES experimental work of MnO^- [92], four low-lying states which are relevant to the detachments of $9\sigma_\beta$, $4\pi_\alpha$, $9\sigma_\alpha$ and $3\pi_\beta$ -electrons are identified in its spectral assignment with the Δ -SCF calculations for the anion ground state ${}^5\Sigma^+$. However, we only include $9\sigma_\beta$ and $3\pi_\beta$ -orbitals into the TMO27 testset for the sake of reliability, whereas $9\sigma_\alpha$ and $4\pi_\alpha$ -orbitals are excluded. This is because the relative ordering of $4\pi_\alpha$ and $9\sigma_\alpha$ -orbitals is rather controversial in the theoretical calculations: At the mean-field level, both PBE0 and B3LYP produce almost the same IEs for $4\pi_\alpha$ and $9\sigma_\alpha$ -electrons. By contrast, G_0W_0 gives a 0.10 eV separation with the $9\sigma_\alpha$ -orbital lying below in energy, whereas $G_0W_0\Gamma_0^{(1)}$ and $G_0W_0+\text{SOSEX}$ predict a 0.05 ~ 0.3 eV splitting with a reversed ordering. This makes the assignment of the IEs of $4\pi_\alpha$ and $9\sigma_\alpha$ -electrons highly unreliable. On the other hand, spectral features at 1.38 eV and 3.58 eV, each with large separation from its adjacent peaks, can be unambiguously assigned to the detachments of $9\sigma_\beta$ and $3\pi_\beta$ -electrons, supported by the calculation results.

3. CoO^-

There is a controversy about the ground state of CoO^- , i.e., whether it's the low-spin state ${}^3\Sigma^-$ ($9\sigma^2 1\delta^4 4\pi^2$) [61] or

the high-spin state ${}^5\Delta$ ($10\sigma^1 9\sigma^2 1\delta^3 4\pi^2$) [99, 105]. Our own spin-unrestricted structural relaxation with the PBE functional indicates that the ${}^3\Sigma^-$ state as the ground state of CoO^- . In Refs. [78, 106], the anion PES data of CoO^- was reported, but no detailed assignment is provided. Here we provide a spectral assignment based on their experimental results and our own calculation work (see Table VI). It should be mentioned that, Zheng *et al.* [78] assign the first strong X peak at 1.54 ± 0.04 eV as the EA of CrO , which is quite different from previous two PES experimental work [107, 108] who recognize the peak at 1.45 ± 0.01 eV as the EA. Instead, Zheng *et al.* regard the peak at 1.45 eV (which has been observed in the 532 nm spectrum in their work) as a hot band, while this feature in fact becomes as strong as the X peak in the 266 nm spectrum [78]. Combining the calculation results in this work, we conclude that the peak at 1.45 eV corresponds to the one-electron detachment of the $1\delta_\beta$ -electron from the anion ground state ${}^3\Sigma^-$, and the final state ${}^4\Delta$ is exactly the ground state of the neutral CoO .

TABLE VI. Ionization energies (in eV) of low-lying states in CoO^- with the anion ground state established as ${}^3\Sigma^-$ ($9\sigma^2 1\delta^4 4\pi^2$).

Final state	${}^4\Delta$	${}^4\Sigma^-$	${}^2\Sigma^+$	${}^2\Pi$
MO	$1\delta_\beta$	$9\sigma_\beta$	$9\sigma_\alpha$	$4\pi_\alpha$
Expt ^a	1.45	1.54	2.17	2.30
PBE0	0.37	-0.12	1.22	1.22
	@PBE0			
G_0W_0	1.23	1.30	2.37	2.33
$G_0W_0+\text{SOSEX}$	2.21	-	2.66	2.79
$G_0W_0\Gamma_0^{(1)}$	1.95	1.80	2.67	2.69
B3LYP	-0.08	-0.27	0.87	0.93
	@B3LYP			
G_0W_0	0.84	1.15	2.01	2.03
$G_0W_0+\text{SOSEX}$	1.89	-	2.26	2.46
$G_0W_0\Gamma_0^{(1)}$	1.50	1.68	2.27	2.36

^a Ref. [78].

[1] L. Hedin, New method for calculating the one-particle Green's function with application to the electron-gas problem, *Phys. Rev.* **139**, A796 (1965).

[2] F. Aryasetiawan and O. Gunnarsson, The GW method, *Rep. Prog. Phys.* **61**, 237 (1998).

- [3] L. Reining, The *GW* approximation: Content, successes and limitations, *WIREs Comput. Mol. Sci.* **8**, e1344 (2018).
- [4] P. Hohenberg and W. Kohn, Inhomogeneous electron gas, *Phys. Rev.* **136**, B864 (1964).
- [5] W. Kohn and L. J. Sham, Self-consistent equations including exchange and correlation effects, *Phys. Rev.* **140**, A1133 (1965).
- [6] A. Seidl, A. Görling, P. Vogl, J. A. Majewski, and M. Levy, Generalized Kohn-Sham schemes and the band-gap problem, *Phys. Rev. B* **53**, 3764 (1996).
- [7] M. S. Hybertsen and S. G. Louie, First-principles theory of quasiparticles: Calculation of band gaps in semiconductors and insulators, *Phys. Rev. Lett.* **55**, 1418 (1985).
- [8] M. S. Hybertsen and S. G. Louie, Electron correlation in semiconductors and insulators: Band gaps and quasiparticle energies, *Phys. Rev. B* **34**, 5390 (1986).
- [9] R. W. Godby, M. Schlüter, and L. J. Sham, Self-energy operators and exchange-correlation potentials in semiconductors, *Phys. Rev. B* **37**, 10159 (1988).
- [10] G. Onida, L. Reining, and A. Rubio, Electronic excitations: density-functional versus many-body Green's-function approaches, *Rev. Mod. Phys.* **74**, 601 (2002).
- [11] X. Blase, C. Attaccalite, and V. Olevano, First-principles *GW* calculations for fullerenes, porphyrins, phthalocyanine, and other molecules of interest for organic photovoltaic applications, *Phys. Rev. B* **83**, 115103 (2011).
- [12] D. Golze, L. Keller, and P. Rinke, Accurate absolute and relative core-level binding energies from *GW*, *J. Phys. Chem. Lett.* **11**, 1840 (2020).
- [13] M. J. van Setten, F. Caruso, S. Sharifzadeh, X. Ren, M. Scheffler, F. Liu, J. Lischner, L. Lin, J. R. Deslippe, S. G. Louie, C. Yang, F. Weigend, J. B. Neaton, F. Evers, and P. Rinke, *GW*100: Benchmarking G_0W_0 for molecular systems, *J. Chem. Theory Comput.* **11**, 5665 (2015).
- [14] F. Bruneval and M. A. L. Marques, Benchmarking the starting points of the *GW* approximation for molecules, *J. Chem. Theory Comput.* **9**, 324 (2013).
- [15] J. W. Knight, X. Wang, L. Gallandi, O. Dolgounitcheva, X. Ren, J. V. Ortiz, P. Rinke, T. Körzdörfer, and N. Marom, Accurate ionization potentials and electron affinities of acceptor molecules III: A benchmark of *GW* methods, *J. Chem. Theory Comput.* **12**, 615 (2016).
- [16] N. Marom, F. Caruso, X. Ren, O. T. Hofmann, T. Körzdörfer, J. R. Chelikowsky, A. Rubio, M. Scheffler, and P. Rinke, Benchmark of *GW* methods for azabenzene, *Phys. Rev. B* **86**, 245127 (2012).
- [17] P. Romaniello, S. Guyot, and L. Reining, The self-energy beyond *GW*: Local and nonlocal vertex corrections, *J. Chem. Phys.* **131**, 154111 (2009).
- [18] W. Nelson, P. Bokes, P. Rinke, and R. W. Godby, Self-interaction in Green's-function theory of the hydrogen atom, *Phys. Rev. A* **75**, 032505 (2007).
- [19] Y. Jin, N. Q. Su, and W. Yang, Renormalized singles Green's function for quasi-particle calculations beyond the G_0W_0 approximation, *J. Phys. Chem. Lett.* **10**, 447 (2019).
- [20] M. Gatti, F. Bruneval, V. Olevano, and L. Reining, Understanding correlations in vanadium dioxide from first principles, *Phys. Rev. Lett.* **99**, 266402 (2007).
- [21] L. I. Bendavid and E. A. Carter, Status in calculating electronic excited states in transition metal oxides from first principles, in *First Principles Approaches to Spectroscopic Properties of Complex Materials*, edited by C. Di Valentin, S. Botti, and M. Cococcioni (Springer Berlin Heidelberg, Berlin, Heidelberg, 2014) pp. 47–98.
- [22] C. Rödl, F. Fuchs, J. Furthmüller, and F. Bechstedt, Quasiparticle band structures of the antiferromagnetic transition-metal oxides MnO, FeO, CoO, and NiO, *Phys. Rev. B* **79**, 235114 (2009).
- [23] H. Jiang, R. I. Gomez-Abal, P. Rinke, and M. Scheffler, First-principles modeling of localized *d* states with the *GW@LDA+U* approach, *Phys. Rev. B* **82**, 045108 (2010).
- [24] F. Fuchs, J. Furthmüller, F. Bechstedt, M. Shishkin, and G. Kresse, Quasiparticle band structure based on a generalized Kohn-Sham scheme, *Phys. Rev. B* **76**, 115109 (2007).
- [25] C. Rödl, F. Sottile, and L. Reining, Quasiparticle excitations in the photoemission spectrum of CuO from first principles: A *GW* study, *Phys. Rev. B* **91**, 045102 (2015).
- [26] M. Grumet, P. Liu, M. Kaltak, J. Klimeš, and G. Kresse, Beyond the quasiparticle approximation: Fully self-consistent *GW* calculations, *Phys. Rev. B* **98**, 155143 (2018).
- [27] B. Holm and U. von Barth, Fully self-consistent *GW* self-energy of the electron gas, *Phys. Rev. B* **57**, 2108 (1998).
- [28] W.-D. Schöne and A. G. Eguiluz, Self-consistent calculations of quasiparticle states in metals and semiconductors, *Phys. Rev. Lett.* **81**, 1662 (1998).
- [29] P.-F. Loos, P. Romaniello, and J. A. Berger, Green functions and self-consistency: Insights from the spherium model, *J. Chem. Theory Comput.* **14**, 3071 (2018).
- [30] F. Caruso, P. Rinke, X. Ren, M. Scheffler, and A. Rubio, Unified description of ground and excited states of finite systems: The self-consistent *GW* approach, *Phys. Rev. B* **86**, 081102 (2012).
- [31] F. Caruso, P. Rinke, X. Ren, A. Rubio, and M. Scheffler, Self-consistent *GW*: All-electron implementation with localized basis functions, *Phys. Rev. B* **88**, 075105 (2013).
- [32] P. Koval, D. Foerster, and D. Sánchez-Portal, Fully self-consistent *GW* and quasiparticle self-consistent *GW* for molecules, *Phys. Rev. B* **89**, 155417 (2014).
- [33] F. Caruso, M. Dauth, M. J. van Setten, and P. Rinke, Benchmark of *GW* approaches for the *GW*100 test set, *J. Chem. Theory Comput.* **12**, 5076 (2016).
- [34] R. T. M. Ummels, P. A. Bobbert, and W. van Haeringen, First-order corrections to random-phase approximation *GW* calculations in silicon and diamond, *Phys. Rev. B* **57**, 11962 (1998).
- [35] E. L. Shirley, Self-consistent *GW* and higher-order calculations of electron states in metals, *Phys. Rev. B* **54**, 7758 (1996).
- [36] A. Grüneis, G. Kresse, Y. Hinuma, and F. Oba, Ionization potentials of solids: The importance of vertex corrections, *Phys. Rev. Lett.* **112**, 096401 (2014).
- [37] Y. Pavlyukh, A.-M. Uimonen, G. Stefanucci, and R. van Leeuwen, Vertex corrections for positive-definite spectral functions of simple metals, *Phys. Rev. Lett.* **117**, 206402 (2016).
- [38] C. Mejuto-Zaera, G. Weng, M. Romanova, S. J. Cotton, K. B. Whaley, N. M. Tubman, and V. Vlček, Are multi-quasiparticle interactions important in molecular ionization?, *J. Chem. Phys.* **154**, 121101 (2021).
- [39] A. Förster and L. Visscher, Exploring the statically screened G_3W_2 correction to the *GW* self-energy: Charged excitations and total energies of finite systems, *Phys. Rev. B* **105**, 125121 (2022).
- [40] F. Bruneval, F. Sottile, V. Olevano, R. Del Sole, and L. Reining, Many-body perturbation theory using the density-functional concept: Beyond the *GW* approximation, *Phys. Rev. Lett.* **94**, 186402 (2005).
- [41] A. M. Lewis and T. C. Berkelbach, Vertex corrections to the polarizability do not improve the *GW* approximation for the

- ionization potential of molecules, *J. Chem. Theory Comput.* **15**, 2925 (2019).
- [42] X. Ren, N. Marom, F. Caruso, M. Scheffler, and P. Rinke, Beyond the *GW* approximation: A second-order screened exchange correction, *Phys. Rev. B* **92**, 081104(R) (2015).
- [43] E. Maggio and G. Kresse, *GW* vertex corrected calculations for molecular systems, *J. Chem. Theory Comput.* **13**, 4765 (2017).
- [44] Y. Wang, P. Rinke, and X. Ren, Assessing the $G_0W_0\Gamma_0^{(1)}$ approach: Beyond G_0W_0 with Hedin's full second-order self-energy contribution, *J. Chem. Theory Comput.* **17**, 5140 (2021).
- [45] A. L. Kutepov, Electronic structure of Na, K, Si, and LiF from self-consistent solution of Hedin's equations including vertex corrections, *Phys. Rev. B* **94**, 155101 (2016).
- [46] M. Hellgren, N. Colonna, and S. de Gironcoli, Beyond the random phase approximation with a local exchange vertex, *Phys. Rev. B* **98**, 045117 (2018).
- [47] M. Shishkin, M. Marsman, and G. Kresse, Accurate quasiparticle spectra from self-consistent *GW* calculations with vertex corrections, *Phys. Rev. Lett.* **99**, 246403 (2007).
- [48] R. Kuwahara, Y. Noguchi, and K. Ohno, *GW* Γ +Bethe-Salpeter equation approach for photoabsorption spectra: Importance of self-consistent *GW* Γ calculations in small atomic systems, *Phys. Rev. B* **94**, 121116 (2016).
- [49] A. Tal, W. Chen, and A. Pasquarello, Vertex function compliant with the Ward identity for quasiparticle self-consistent calculations beyond *GW*, *Phys. Rev. B* **103**, L161104 (2021).
- [50] B. Cunningham, M. Gruening, D. Pashov, and M. van Schilf-gaarde, *QSGW*: Quasiparticle self consistent *GW* with ladder diagrams in *W* (2021), [arXiv:2106.05759](https://arxiv.org/abs/2106.05759) [cond-mat.mtrl-sci].
- [51] A. L. Kutepov, Self-consistent solution of Hedin's equations: Semiconductors and insulators, *Phys. Rev. B* **95**, 195120 (2017).
- [52] M. Mansouri, D. Casanova, P. Koval, and D. Sánchez-Portal, *GW* approximation for open-shell molecules: a first-principles study, *New J. Phys.* **23**, 093027 (2021).
- [53] S. Körbel, P. Boulanger, I. Duchemin, X. Blase, M. A. L. Marques, and S. Botti, Benchmark many-body *GW* and Bethe-Salpeter calculations for small transition metal molecules, *J. Chem. Theory Comput.* **10**, 3934 (2014).
- [54] L. Hung, F. Bruneval, K. Baishya, and S. Ögüt, Benchmarking the *GW* approximation and Bethe-Salpeter equation for groups IB and IIB atoms and monoxides, *J. Chem. Theory Comput.* **13**, 2135 (2017).
- [55] B. Shi, S. Weissman, F. Bruneval, L. Kronik, and S. Ögüt, Photoelectron spectra of copper oxide cluster anions from first principles methods, *J. Chem. Phys.* **149**, 064306 (2018).
- [56] M. Rezaei and S. Ögüt, Photoelectron spectra of early 3*d*-transition metal dioxide molecular anions from *GW* calculations, *J. Chem. Phys.* **154**, 094307 (2021).
- [57] K. T. Williams, Y. Yao, J. Li, L. Chen, H. Shi, M. Motta, C. Niu, U. Ray, S. Guo, R. J. Anderson, J. Li, L. N. Tran, C.-N. Yeh, B. Mussard, S. Sharma, F. Bruneval, M. van Schilf-gaarde, G. H. Booth, G. K.-L. Chan, S. Zhang, E. Gull, D. Zgid, A. Millis, C. J. Umrigar, and L. K. Wagner (Simons Collaboration on the Many-Electron Problem), Direct comparison of many-body methods for realistic electronic hamiltonians, *Phys. Rev. X* **10**, 011041 (2020).
- [58] Y.-M. Byun and S. Ögüt, Practical *GW* scheme for electronic structure of 3*d*-transition-metal monoxide anions: ScO^- , TiO^- , CuO^- , and ZnO^- , *J. Chem. Phys.* **151**, 134305 (2019).
- [59] C. W. Bauschlicher and P. M. Jr., Theoretical study of the first transition row oxides and sulfides, *Theoret. Chim. Acta* **90**, 189 (1995).
- [60] A. J. Merer, Spectroscopy of the diatomic 3*d* transition metal oxides, *Annu. Rev. Phys. Chem.* **40**, 407 (1989).
- [61] G. L. Gutsev, B. K. Rao, and P. Jena, Electronic structure of the 3*d* metal monoxide anions, *J. Phys. Chem. A* **104**, 5374 (2000).
- [62] J. F. Harrison, Electronic structure of diatomic molecules composed of a first-row transition metal and main-group element (H-F), *Chem. Rev.* **100**, 679 (2000).
- [63] Y. Gong, M. Zhou, and L. Andrews, Spectroscopic and theoretical studies of transition metal oxides and dioxygen complexes, *Chem. Rev.* **109**, 6765 (2009).
- [64] J. Fan and L. Wang, Photoelectron spectroscopy of FeO^- and FeO_2^- : Observation of low-spin excited states of FeO and determination of the electron affinity of FeO_2 , *J. Chem. Phys.* **102**, 8714 (1995).
- [65] M. F. A. Hendrickx and K. R. Anam, A new proposal for the ground state of the FeO^- cluster in the gas phase and for the assignment of its photoelectron spectra, *J. Phys. Chem. A* **113**, 8746 (2009).
- [66] J. B. Kim, M. L. Weichman, and D. M. Neumark, Low-lying states of FeO and FeO^- by slow photoelectron spectroscopy, *Mol. Phys.* **113**, 2105 (2015).
- [67] C. N. Sakellaris, E. Miliordos, and A. Mavridis, First principles study of the ground and excited states of FeO, FeO^+ , and FeO^- , *J. Chem. Phys.* **134**, 234308 (2011).
- [68] C. W. Bauschlicher and S. R. Langhoff, Theoretical studies of the low-lying states of ScO, ScS, VO, and VS, *J. Chem. Phys.* **85**, 5936 (1986).
- [69] E. Miliordos and A. Mavridis, Electronic structure and bonding of the early 3*d*-transition metal diatomic oxides and their ions: $\text{ScC}^{0,\pm}$, $\text{TiO}^{0,\pm}$, $\text{CrO}^{0,\pm}$, and $\text{MnO}^{0,\pm}$, *J. Phys. Chem. A* **114**, 8536 (2010).
- [70] M. Pykavy and C. van Wüllen, Multireference correlation calculations for the ground states of $\text{VO}^{0,\pm}$ using correlation consistent basis sets, *J. Phys. Chem. A* **107**, 5566 (2003).
- [71] P. S. Bagus, C. J. Nelin, and C. W. Bauschlicher, On the low-lying states of CuO, *J. Chem. Phys.* **79**, 2975 (1983).
- [72] C. N. Sakellaris, A. Papakonodylis, and A. Mavridis, Ab initio study of the electronic structure of zinc oxide and its ions, $\text{ZnO}^{0,\pm}$ ground and excited states, *J. Phys. Chem. A* **114**, 9333 (2010).
- [73] B. Dai, K. Deng, J. Yang, and Q. Zhu, Excited states of the 3*d* transition metal monoxides, *J. Chem. Phys.* **118**, 9608 (2003).
- [74] H. J. Kulik and N. Marzari, Systematic study of first-row transition-metal diatomic molecules: A self-consistent DFT+*U* approach, *J. Chem. Phys.* **133**, 114103 (2010).
- [75] H. Wu and L.-S. Wang, Photoelectron spectroscopy and electronic structure of ScO_n^- ($n = 1 - 4$) and YO_n^- ($n = 1 - 5$): Strong electron correlation effects in ScO^- and YO^- , *J. Phys. Chem. A* **102**, 9129 (1998).
- [76] H. Wu and L.-S. Wang, Electronic structure of titanium oxide clusters: TiO_y ($y = 1 - 3$) and $(\text{TiO}_2)_n$ ($n = 1 - 4$), *J. Chem. Phys.* **107**, 8221 (1997).
- [77] H. Wu and L.-S. Wang, A photoelectron spectroscopic study of monovanadium oxide anions (VO_x^- , $x = 1 - 4$), *J. Chem. Phys.* **108**, 5310 (1998).
- [78] R.-Z. Li, J. Liang, X.-L. Xu, H.-G. Xu, and W.-J. Zheng, Photoelectron spectroscopy and density functional theory study of Co_nO^- ($n = 1 - 3$), *Chem. Phys. Lett.* **575**, 12 (2013).
- [79] H. Wu and L.-S. Wang, A study of nickel monoxide (NiO), nickel dioxide (ONiO), and Ni(O₂) complex by anion photo-

- electron spectroscopy, *J. Chem. Phys.* **107**, 16 (1997).
- [80] H. Wu, S. R. Desai, and L.-S. Wang, Chemical bonding between Cu and oxygen-copper oxides vs O₂ complexes: A study of CuO_x ($x = 0 - 6$) species by anion photoelectron spectroscopy, *J. Phys. Chem. A* **101**, 2103 (1997).
- [81] J. H. Kim, X. Li, L.-S. Wang, H. L. de Clercq, C. A. Fancher, O. C. Thomas, and K. H. Bowen, Vibrationally resolved photoelectron spectroscopy of MgO⁻ and ZnO⁻ and the low-lying electronic states of MgO, MgO⁻, and ZnO, *J. Phys. Chem. A* **105**, 5709 (2001).
- [82] V. D. Moravec, S. A. Klopčič, B. Chatterjee, and C. C. Jarrold, The electronic structure of ZnO and ZnF determined by anion photoelectron spectroscopy, *Chem. Phys. Lett.* **341**, 313 (2001).
- [83] J. P. Perdew, K. Burke, and M. Ernzerhof, Generalized gradient approximation made simple, *Phys. Rev. Lett.* **77**, 3865 (1996).
- [84] C. Adamo and V. Barone, Toward reliable density functional methods without adjustable parameters: The PBE0 model, *J. Chem. Phys.* **110**, 6158 (1999).
- [85] A. D. Becke, Density-functional thermochemistry. III. The role of exact exchange, *J. Chem. Phys.* **98**, 5648 (1993).
- [86] P. J. Stephens, F. J. Devlin, C. F. Chabalowski, and M. J. Frisch, Ab initio calculation of vibrational absorption and circular dichroism spectra using density functional force fields, *J. Phys. Chem.* **98**, 11623 (1994).
- [87] T. H. Dunning, Gaussian basis sets for use in correlated molecular calculations. I. the atoms boron through neon and hydrogen, *J. Chem. Phys.* **90**, 1007 (1989).
- [88] X. Ren, P. Rinke, V. Blum, J. Wieferink, A. Tkatchenko, A. Sanfilippo, K. Reuter, and M. Scheffler, Resolution-of-identity approach to Hartree-Fock, hybrid density functionals, RPA, MP2 and GW with numeric atom-centered orbital basis functions, *New J. Phys.* **14**, 053020 (2012).
- [89] G. A. Baker, in *Essentials of Padé Approximants* (Academic Press, New York, 1975) Chap. 8, p. 105.
- [90] V. Blum, R. Gehrke, F. Hanke, P. Havu, V. Havu, X. Ren, K. Reuter, and M. Scheffler, Ab initio molecular simulations with numeric atom-centered orbitals, *Comput. Phys. Commun.* **180**, 2175 (2009).
- [91] G. L. Gutsev, P. Jena, H.-J. Zhai, and L.-S. Wang, Electronic structure of chromium oxides, CrO_n⁻ and CrO_n ($n = 1-5$) from photoelectron spectroscopy and density functional theory calculations, *J. Chem. Phys.* **115**, 7935 (2001).
- [92] G. L. Gutsev, B. K. Rao, P. Jena, X. Li, and L.-S. Wang, Experimental and theoretical study of the photoelectron spectra of MnO_x⁻ ($x = 1 - 3$) clusters, *J. Chem. Phys.* **113**, 1473 (2000).
- [93] H. Wu, S. R. Desai, and L.-S. Wang, Observation and photoelectron spectroscopic study of novel mono- and diiron oxide molecules: FeO_y⁻ ($y = 1 - 4$) and Fe₂O_y⁻ ($y = 1 - 5$), *J. Am. Chem. Soc.* **118**, 5296 (1996).
- [94] N. Marom, X. Ren, J. E. Moussa, J. R. Chelikowsky, and L. Kronik, Electronic structure of copper phthalocyanine from *G*₀*W*₀ calculations, *Phys. Rev. B* **84**, 195143 (2011).
- [95] T. Jiang, Y. Chen, N. A. Bogdanov, E. Wang, A. Alavi, and J. Chen, A full configuration interaction quantum Monte Carlo study of ScO, TiO, and VO molecules, *J. Chem. Phys.* **154**, 164302 (2021).
- [96] T. Andersen, K. R. Lykke, D. M. Neumark, and W. C. Lineberger, Autodetachment study of the electronic spectroscopy of FeO⁻, *J. Chem. Phys.* **86**, 1858 (1987).
- [97] G. Drechsler, U. Boesl, C. BäSmann, and E. W. Schlag, Mass selected anion-zero kinetic energy photoelectron spectroscopy (anion-ZEKE): Ground and low excited states of FeO, *J. Chem. Phys.* **107**, 2284 (1997).
- [98] G. L. Gutsev, S. N. Khanna, B. K. Rao, and P. Jena, Electronic structure and properties of FeO_n and FeO_n⁻ clusters, *J. Phys. Chem. A* **103**, 5812 (1999).
- [99] E. L. Uzunova, H. Mikosch, and G. S. Nikolov, Electronic structure of oxide, peroxide, and superoxide clusters of the 3d elements: A comparative density functional study, *J. Chem. Phys.* **128**, 094307 (2008).
- [100] M. Krauss and W. J. Stevens, Electronic structure of feo and ruo, *J. Chem. Phys.* **82**, 5584 (1985).
- [101] P. C. Engelking and W. C. Lineberger, Laser photoelectron spectrometry of FeO⁻: Electron affinity, electronic state separations, and ground state vibrations of iron oxide, and a new ground state assignment, *J. Chem. Phys.* **66**, 5054 (1977).
- [102] S.-B. Cheng, C. L. Harmon, H. Yang, and A. W. Castleman, Electronic structure of the diatomic VO anion: A combined photoelectron-imaging spectroscopic and theoretical investigation, *Phys. Rev. A* **94**, 062506 (2016).
- [103] A. Merer, G. Huang, A.-C. Cheung, and A. Taylor, New quartet and doublet electronic transitions in the near-infrared emission spectrum of VO, *J. Mol. Spectrosc.* **125**, 465 (1987).
- [104] C. W. Bauschlicher and G. L. Gutsev, A new interpretation of the CrO⁻ photoelectron detachment spectra, *J. Chem. Phys.* **116**, 3659 (2002).
- [105] C. N. Sakellaris and A. Mavridis, Electronic structure and bonding of cobalt monoxide, CoO, and its ions CoO⁺ and CoO⁻: An ab initio study, *J. Phys. Chem. A* **116**, 6935 (2012).
- [106] R.-Z. Li, H.-G. Xu, G.-J. Cao, Y.-C. Zhao, and W.-J. Zheng, Interaction of Co_mO⁻ ($m = 1 - 3$) with water: Anion photoelectron spectroscopy and density functional calculations, *J. Chem. Phys.* **135**, 134307 (2011).
- [107] A. G. Adam, Y. Azuma, J. A. Barry, G. Huang, M. P. J. Lyne, A. J. Merer, and J. O. Schröder, A laser-induced fluorescence study of bands of the red system of gaseous CoO: Evidence for a ⁴δ_i ground state, *J. Chem. Phys.* **86**, 5231 (1987).
- [108] X. Li and L.-S. Wang, Electronic structure and chemical bonding between the first row transition metals and C₂: A photoelectron spectroscopy study of MC₂⁻ (M=Sc, V, Cr, Mn, Fe, and Co), *J. Chem. Phys.* **111**, 8389 (1999).